Article

# Dominance of Broken Bonds and Unpaired Nonbonding #-Electrons in the Band Gap Expansion and Edge States Generation in Graphene Nanoribbons

Chang Q. Sun, Shao-Yun Fu, and Y. G. Nie

*J. Phys. Chem. C*, **2008**, 112 (48), 18927-18934 • Publication Date (Web): 08 November 2008

# Dominance of Broken Bonds and Unpaired Nonbonding $\pi$-Electrons in the Band Gap Expansion and Edge States Generation in Graphene Nanoribbons

**Chang Q. Sun,*,† Shao-Yun Fu,*,‡ and Y. G. Nie†**

*School of Electrical and Electronic Engineering, Nanyang Technological University, Singapore 639798, Singapore, Key Laboratory of Low-dimensional Materials and Application Technology (Ministry of Education), Xiangtan University, Hunan, 411105, China, Technical Institute of Physics and Chemistry, Chinese Academy of Sciences, Beijing 100190*

*Received: August 25, 2008; Revised Manuscript Received: October 3, 2008*

Incorporating the bond-order-length-strength (BOLS) correlation theory [Sun, C. Q. *Prog. Solid State Chem.* **2007**, *35*, 1] to density functional theory calculations and experimental observations has led to consistent insight into the electronic behavior of graphene nanoribbons (GNRs) from the perspective of bond formation, dissociation and relaxation and the associated dynamics and energetics of charge densification, localization, and polarization. The consistency between the BOLS predictions and the observed coordination dependence of bond contraction and the associated thermal instability, mechanical strength, and band structure variation in various situations evidence the significance of the broken bond that induces local strain and quantum trapping. The inconsistency between the theoretically and experimentally observed band gap expansions in GNRs indicates particularly the impact of the unpaired nonbonding (called $\pi$-bond) electrons and the adsorbate-induced inhomogeneous repulsion along the edges. A perturbation to the Hamiltonian by the local strain and edge trapping dictates intrinsically the band structure yet the presence and polarization of the nonbonding states by the nearby densely trapped bonding electrons and the adsorbate-induced inhomogeneous repulsion along the edges dominate the observed edge states.

## I. Introduction

Unrolled single-walled carbon nanotubes (SWCNTs), called graphene nanoribbons (GNRs),[1−3] with open edges have inspired increasing interest recently because of their intriguing properties that cannot be seen from the SWCNTs or the infinitely large graphene sheets (LGSs). Upon hybridization of $sp^2$ orbits, electrons of each carbon atom in the LGS form three $\sigma$ bonds to the neighboring atoms in a $C_{3v}$ symmetry, and the unpaired nonbonding electron of the carbon develops into the $\pi$ and $\pi^*$ states at the corner of the Brillouin zone or below the Dirac point[4] in the midgap region. Generally, the unpaired electrons are responsible for both the conductivity and the weak interactions between the layers of the graphite. The involvement of nonbonding electrons, which distinguishes graphite from diamond in performance, is indeed fascinating. There are typically two types of GNRs, according to the shapes of the edges. One is the armchair-edged AGNR, and the other is the zig-zag-edged ZGNR. When compared with LGSs or CNTs, the ZGNRs possess strongly localized edge states[5] with a metallic nature, whereas the AGNRs have a larger band gap ($E_G$) with a semiconductive nature. The $E_G$ is found roughly proportional to the inverse width of the GNRs.[6−9] It has been found in tight-binding calculations[10] that a relaxation of the edge structure of AGNR is crucial for obtaining a nonmetallic band gap. Conductance calculations have suggested that edge disorder[11] in AGNRs could cause short localization lengths, which could make expected semiconducting GNR devices insulating. A single edge defect could even induce localized states and, consequently, zero-conductance dips.[12] The edge and defect states are therefore critical to the performance of GNRs,[7] despite chemical passivation that may modulate the electronic structures of the edge atoms to a certain extent.[13,14] Electron transport dynamics measurement[8] at temperatures below 200 K revealed that the $E_G$ varies with the GNR width, $W$, as $E_G = \alpha(W - W_0)^{-1}$, with the values of $\alpha = 0.2$ eVnm and $W_0 = 16$ nm. When the GNR is narrower than $W_0$, the $E_G$ increases abruptly to several electron volts and then approaches the values derived from density function theory (DFT) calculations.[6] On the other hand, the unpaired $\pi$-electrons with particular spins are strongly localized at the edges of the ZGNR, with energy being at the Fermi level or above as probed using scanning tunneling microscopy and spectroscopy (STM/S).[15] The edge states give rise to many unusual phenomena, such as the unconventional magnetism that enables the carbon-only ferromagnetism, spin glass state, half-integer quantum Hall effect,[16] ultrahigh electric and thermal mobility,[17] extremely high group velocity and extremely low effective mass, etc.[3−20]

Despite the fascinating phenomena and the promising potentials of applications for the next generation of electronic, optic (THz), and magnetic devices, mechanisms remain yet unclear regarding the generation of the localized edge states and the expansion of the $E_G$, despite possible mechanisms such as doping or defects,[21,22] symmetry breaking,[23] substrate interaction,[24] and quantum confinement.[15] It has been suggested that the $E_G$ opening of AGNRs originates from quantum confinement and edge effect[6] or from edge distortion.[7] The distortion affects the bond lengths and causes truncation of the neighboring interactions that occur because of the strip edges. It has been suggested that the $E_G$ expansion in ZGNRs originates from the staggered sublattice potentials due to the magnetic ordering.[25] Despite the overwhelming contributions made in recent years toward the physical insight into the unusual behavior of GNRs,

* E-mail: ecqsun@ntu.edu.sg; syfu@mail.ipc.ac.cn.
† Nanyang Technological University.
‡ Technical Institute of Physics and Chemistry.

10.1021/jp807580t CCC: $40.75 
Published on Web 11/08/2008

understanding from the perspective of chemical bonding and its effect on valence states is yet lacking. Here, we show with analytical expressions that the broken-bond-induced local strain and quantum trapping and the associated densification of charge and energy results intrinsically in the $E_G$ opening and energy level shift[26] and that the presence and polarization of the unpaired nonbonding states by the densely trapped bonding electrons are responsible for the edge states and the measured $E_G$ values. The difference between ZGNR and AGNR arises from the repulsion induced by hydrogen termination along the edges.

## II. Theory

**2.1. The $E_G$, Core Level Shift, Elastic Modulus and Thermal Stability.** According to the simple tight-binding band theory,[27] the coupling of the interatomic potential, $V_{cry}(r)$, and the respective Bloch wave functions, being proportional to the mean cohesive energy per bond, $\langle E_0 \rangle$, determines the energy band identities as a whole, such as the gap between the conduction and the valence band in semiconductors, $E_G$; the energy dispersion, $E_\nu(k)$; and the energy shift of the specific core band, denoted with subscript $\nu$, $\Delta E_\nu(\infty) = E_\nu(\infty) - E_\nu(1)$, with respect to the corresponding $\nu$th energy level of an isolated atom. The single-body Hamiltonian, $H$, and the related band identities are given as[28]

$$\begin{array}{lll} H & = -\dfrac{\hbar^2\nabla^2}{2m} + V_{atom}(r) + V_{cry}(r) & \text{(Hamiltonian)} \\ E_G(\infty) & = 2|V_h| \propto \langle E_0 \rangle & \text{(band gap)} \\ E_\nu(k) & = E_\nu(1) - \beta - \gamma \sum{}' e^{ik\cdot R_j} & \text{(energy disperison)} \\ E_\nu(1) & = \langle \varphi_\nu(r)|V_{atom}(r)|\varphi_\nu(r)\rangle & \text{(core level energy)} \\ \beta & = \langle \varphi_\nu(r)|V_{cry}(r)|\varphi_\nu(r)\rangle \propto \langle E_0 \rangle & \text{(exchange integral)} \\ \gamma & = \langle \varphi_\nu(r)|V_{cry}(r)|\varphi_\nu(r')\rangle \propto \langle E_0 \rangle & \text{(overlap integral)} \\ \Delta E_\nu(k) & = a\beta + c\gamma \propto \langle E_0 \rangle & \text{(Core level shift)} \\ \Delta E_\nu & \approx \gamma \sum{}' e^{ik\cdot R_j} \propto \langle E_0 \rangle & \text{(Band width)} \end{array} \quad (1)$$

The intra-atomic trapping potential, $V_{atom}(r)$, determines the $\nu$th energy level of an isolated atom, $E_\nu(1)$. The $\phi_\nu(r)(r \neq r')$ is the specific Bloch wave function at a specific site $r$. The $k$ is the wave vector. The $m$ is the mass of an electron. The $E_G$ depends uniquely on the Fourier coefficient of the periodic crystal potential $V_{cry}(r)$, $|V_h|$. The parameters $a$ and $c$ in the $\Delta E_\nu(k)$ are the weighting factors of the sum of the two integrals. The bandwidth depends also on the overlap energy of the neighboring atoms and the geometrical configuration of neighboring atoms, according to the tight-binding theory. Therefore, the interatomic bond energy, $\langle E_0 \rangle$, dominates the entire band structure.

On the other hand, according to the local bond average approach,[29] the elastic modulus and the thermal stability at an atomic site are also related to the bonding parameters in the form of

$$\begin{cases} Y_i \propto d_i^{-3} E_i \\ T_{m,i} \propto z_i E_i \end{cases}$$

with the bulk mean following the relations

$$\begin{cases} \langle Y \rangle & \propto \langle d^{-3} E_0 \rangle \\ \langle T_m \rangle & \propto \langle z E_0 \rangle \end{cases} \quad (2)$$

The relations represent that the $Y$ value at an atomic site is proportional to the energy density and the local melting point is proportional to the atomic cohesive energy. Therefore, the energy band structure, the elastic modulus, and the thermal stability are strongly correlated through the parameters of bond order, length, and strength. Hence, the interatomic potential or the mean bond energy $\langle E_0 \rangle$ forms the key to the band structure, mechanical strength, and thermal properties of a specimen. Without $V_{cry}(r)$, neither the band nor the $E_G$ or the $\Delta E_\nu(k)$ will be generated. The band theory applies to any system, including atomic chains in which $V_{cry}(r) \neq 0$.

Any perturbation to the $V_{cry}(r)$ or to the mean bond energy, $\langle E_0 \rangle$, will modulate the entire band structure and related properties of the given specimen. However, a geometrical orientation alteration of the GNRs could change neither the $E_G$ nor the $\Delta E_\nu(k)$, according to the band theory. One can modify the bond energy by proceeding bond nature alteration through chemical reaction or by proceeding bond relaxation through external stimulus such as changing coordination environment, temperature, or pressure.[26] It is emphasized that the $E_G$ derived from the band theory is intrinsic for ideal crystals without involvement of the nonbonding or antibonding interactions. The nonbonding lone pair states generated by the $sp^3$ hybridization of oxygen and nitrogen and the nonbonding unpaired $\pi$-states in the $sp^2$-hybridized carbon contribute insignificantly to the band framework because the interatomic interactions through such nonbonding or antibonding states are extremely low, with energy around 0.05 eV.[30] However, these nonbonding electrons will form midgap impurity states[31] because the nonbonding electrons neither raise nor lower the energies of the initial $p$ orbitals of the isolated O, N, and C atoms.[32] On the other hand, the nonbonding lone pairs in nitrogen or oxygen will polarize atoms nearby, forming dipoles with electronic states above the Fermi level. The unpaired nonbonding electrons of carbon can be polarized by the nearby $\sigma$-bonding electrons, and the extent of polarization will increase with the density of the bonding electrons. This polarization will raise the energy of the unpaired nonbonding electrons.[33] Extrinsic factors such as the number and the total energy of the electron−hole pairs (excitons) contribute neither to the Hamiltonian nor to the entire band structure. For amorphous, relaxed, or under-ordered systems, the coordination imperfection generates impurity states, adding to the band gap or forming the Ubach edge states at band tails.[31] Charge transition from the midgap impurity or the nonbonding states to the upper band edge gives rise to the apparent $E_G$ that is entirely different from the intrinsic $E_G$ calculated under ideal conditions. Unfortunately, the presence and polarization of the nonbonding states are hardly described from the self-consistent optimization in DFT or tight-binding approximations at the present because of the limitation of interatomic potentials. Potentials suitable for the broken-bond-induced local strain and quantum trapping that are sometimes several folds deeper than the potential at the usual atomic site in the bulk and potentials suitable for the weak interaction between the nonbonding and the polarized antibonding states are highly desirable for computations.

**2.2. BOLS Correlation: Local Strain and Quantum Trapping.** The involvement of the interatomic bonding distinguishes a bulk specimen in performance from the isolated constituent atoms. When compared with the bulk solid, a nanostructure contains large proportion of less-coordinated atoms at edges or surfaces; therefore, interaction between the less-coordinated atoms takes the responsibility for the unusual behavior of nanostructures.[26] The boundary conditions are particularly important in the low-dimensional systems. The GNR is an ideal prototype of two-dimensional nanostructures with the even less-coordinated atoms located at the edges.

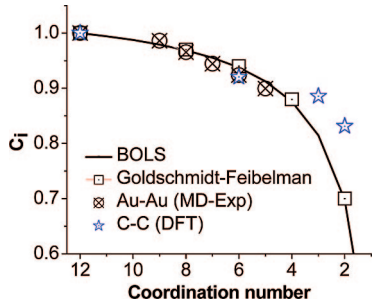


**Figure 1.** Comparison of the BOLS (solid line) prediction with the measured Au−Au[37] and the DFT calculated C−C (this work) bond length as a function of atomic coordination. The CN dependence of Au−Au bond length is in excellent agreement with BOLS prediction. The DFT-calculated C−C bond length follows the trend but does not reach the extent of the BOLS expectations.

According to Goldschmidt,[34] Pauling,[35] and Feibelman,[36] an atom will shrink its radius once the effective coordination number (CN) of the specific atom is reduced. The CN dependence of atomic size is independent of element, bond nature, or phase structure. As illustrated in Figure 1, if the CN of an atom is reduced from the standard bulk value of 12 to 8, 6, 4, and 2, the atomic radius will shrink by 3%, 4%, 12%, and 30%, respectively, according to Goldschmidt−Pauling−Feibelman (GPF) convention.[34,36]

Since 1927, when Goldschmidt first noted the CN dependence of atomic radius shrinkage, little attention has been paid to the effect of atomic CN-induced bond contraction and, particularly, the energetic response of the spontaneous process of bond contraction that should follow the principle of minimum energy. An attempt has been made by this group since 1997 to extend the GPF convention to cover the energetics of the spontaneous process of bond relaxation, which has led to the currently employed bond-order-length-strength (BOLS) correlation as an additional angle of inspection to classical and quantum approximations.

Increasing experimental evidence has been reported to favor the quantitative reliability of the BOLS expectation. For instance, using electron cohesive diffraction, Huang et al.[37] discovered that the Au−Au bond contracts with CN reduction, as plotted in Figure 1 and that the bond contraction happens only to the outermost two atomic layers of a gold nanosolid in a radial way, yet the Au−Au bond in the core interior of the particle retains its bulk value. The CN dependence of Au−Au bond contraction is insensitive to the type of substrate support.[38] These findings agree exceedingly well with the BOLS expectation.

The BOLS correlation can be formulated as[26]

$$\begin{cases} C_i = d_i/d_0 = \\ \quad 2\{1+\exp[(12-z_i)/(8z_i)]\}^{-1} & \text{(bond contraction coefficient)} \\ C_i^{-m} = E_i/E_0 & \text{(bond strengthening coefficient quantum trapping coefficient)} \end{cases} \tag{3}$$

The coefficient of quantum trapping is the same as that for the bond strengthening. The $E_0$ corresponds to the bond energy at equilibrium atomic separation, $d_0$, which is independent of the particular shape of pairing atomic potential. Subscript $i$ represents the specific $i$th atom with $z_i$ coordinates. Superscript $m$ is the bond nature indicator, which has been optimized as 2.56 for carbon nanotubes.[39] The $m$ value may change with atomic CN, such as the atomic clusters composing the III-A and IV-A elements,[40] which is described using a Fermi-type switching function, $m = m_0 + m_1/[1 + \exp(z - z_0)/z_1]$. This relation represents that the $m$ value changes from $m_0$ to $m_0 + m_1/2$ at $z_0$; $z_1$ is the decay length of the $z$-dependence of the $m$ value. It has been found in reproducing the size-induced overheating (melting at temperatures higher than the corresponding bulk melting points) of Ga, Sn, Si, and Al atomic clusters that the $m$ value approaches 7 or higher. The coordination dependence of the $m$ value indicates that the cohesive energy of such less-coordinated atoms is even higher than that in the bulk situation. Nevertheless, we can consider in practice the factor $C_i^{-m}$ as a whole to represent the relative depth of the interatomic potential or the relative strength of the shortened bond without necessarily discriminating the contribution of bond length contraction from the bond nature alteration. It is worth emphasizing that in the BOLS theory analysis, we need to consider only the bond length and bond energy for the statistic properties instead of the particular shape of the interatomic potential, as the self-consistent optimization does in quantum computations.

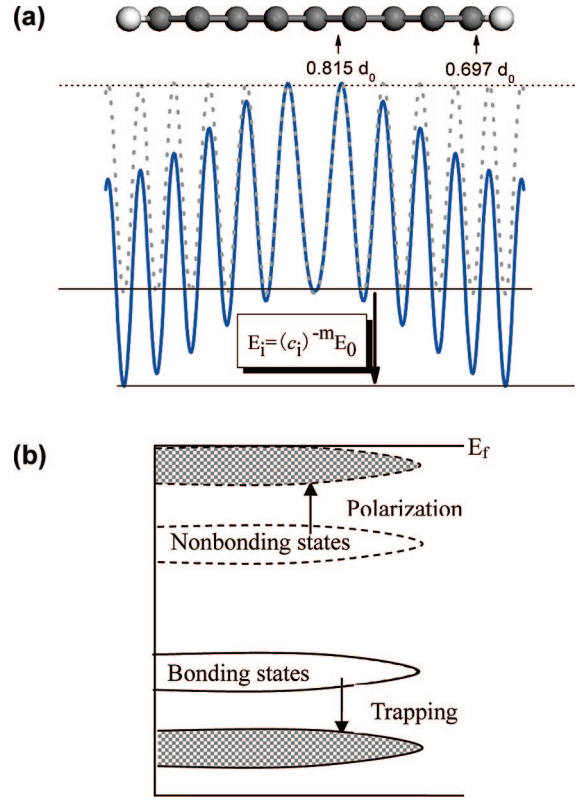


**Figure 2.** (a) Schematic illustration of the BOLS-derived strain and quantum trapping in a $k = 9$ GNR (the cross section is shown), where $d_0$ and $E_0$ are the bond length and energy of diamond. The potential well of trapping is deepened by $C_i^{-m}$ and narrowed at the edges by $C_i$ with respect to that of a diamond. (b) Suggested mechanism for the generation of the localized GNR edge states as arising from the polarization of the unpaired nonbonding states by the densely and deeply trapped $\sigma$-bonding electrons of carbon.

The BOLS correlation mechanism indicates that if one bond breaks, the remaining neighboring ones become shorter and stronger. Consequently, the local strain (bond contraction) and quantum trapping (bond strength gain or potential well depression) surrounding the under-coordinated atoms will cause densification of charge, energy, and mass near the defects. The localized densification is proportional to the

inverse of the bond length of the GNRs. On the other hand, the bond energy gain means the depression of the interatomic potential. Consequently, all the energy levels of the system will shift positively (deeper) by $C_i^{-m}$ with respect to the corresponding bulk values.[28]

As illustrated in Figure 2a, the broken-bond-induced perturbation to the potential energy at the $i$th atomic site is given as

$$V(r_i) = V_{\text{atom}}(r) + V_{\text{cry}}(r)[1 + \Delta_i]$$
$$\Delta_i = \frac{E_i - E_0}{E_0} = C_i^{-m} - 1 \quad (4)$$

$\Delta_i$ is the BOLS perturbation. It is emphasized that the $E_G$ expansion, core level shift, and bandwidth broadening happen simultaneously. Combining eqs 1 and 3, we can readily obtain the following relations[26,28] at atomic scale.

$$\begin{cases} E_G(\Delta_i) & = E_G(\infty)(1 + \Delta_i) \quad \text{(band gap expansion)} \\ \Delta E_{\nu,\text{NGR}} & = \Delta E_{\nu,\text{NGR}}(1 + \Delta_i) \quad \text{(band width expansion)} \\ E_\nu(\Delta_i) - E_\nu(1) & = [E_\nu(\infty) - E_\nu(1)](1 + \Delta_i) \quad \text{(core level shift)} \end{cases} \quad (5)$$

By applying the core−shell configuration for nanostructures[26] to the GNR, we can obtain the width dependence of the $\Delta E_G$, $\Delta E_{\nu,\text{NGR}}$, and $\Delta E_\nu(K)$ of the GNR with respect to that of the LGS by summing over atoms crossing a GNR of infinite length and K width,

$$\frac{\Delta E_G(K)}{E_G(\infty)} = \frac{\Delta E_{\nu,\text{NGR}}}{\Delta E_{\nu,\text{LGS}}} = \frac{E_\nu(K) - E_\nu(1)}{E_\nu(\infty) - E_\nu(1)} = \sum_{i \le 3} \gamma_i \Delta_i = \frac{1}{K} \sum_{i \le 3} C_i (C_i^{-m} - 1) \quad (6)$$

where $\gamma_i = C_i/K$, a weighting factor, is the ratio between the edge of $d_i$ width and the half-width of the GNR. $K$, the dimensionless form of GNR width, is the number of atoms lined across the half-width of the GNR. This relation indicates that the quantum trapping coefficient, $C_i^{-m} - 1$, originates the size-induced change of the entire band structure, including the band gap, core level shift, and the bandwidth, yet the ratio $\gamma_i$ determines the extent of change. If $C_i = 1$, nothing will happen. If $K$ approaches infinity, the relative changes of the band structure for the GNR to that of the LGS are negligible. Here, we take the LGS as the reference of which the band structure will change with respect to the bulk diamond in the ideal situation, as will be discussed shortly.

## III. DFT Calculations

The DFT calculations were conducted using the DMOL$^3$ code with a double numeric plus polarization basis set.[41] Geometric and electronic structures of various carbon allotropes were obtained on the basis of the generalized gradient approximation in the Perdew−Burke−Ernzerh form of potential.[42] During calculations, the self-consistency threshold of total energy was set at $10^{-6}$ au. The tolerance limit for the forces in geometry optimizations was set at $10^{-8}$ au. Calculations were focused on the coordination dependence of C−C bond length, the energy states of various carbon allotropies, and the GNR width dependence of band gap expansion.

## IV. Results and Discussion

**4.1. Coordination Dependence of Bond Contraction.** Figure 1 compares the DFT-calculated CN dependence of the C−C bond lengths. Table 1 also compares the calculated values with the BOLS predictions. The CN's changing from 12 to 6, 3, and 2 corresponds to atoms in a diamond, graphite, GNR interior, GNR edge, or carbon atomic chain, respectively. We take the effective atomic CN in a diamond as 12 instead of 4 because the diamond structure is an interlock of two face-centered-cubic structures.[39] The DFT-optimized C−C bond lengths follow the BOLS predicted trend, but the extent deviates significantly at smaller CN values. The effect of the deviation is enormous because all the quantities discussed herein depend on the extent of bond contraction.

**TABLE 1: Comparison of the BOLS Prediction with the DFT Calculated CN Dependence of C−C Bond Length[a]**

| atomic CN | 12 | 6 | 3 | 2 |
|---|---|---|---|---|
| A (BOLS) | 0.1545 | 0.1449 | 0.1259 | 0.1077 |
| B (DFT) | 0.1547 | 0.1424 | 0.1370 | 0.1286 |

[a] Deviations arising from the artifacts of the DFT package as the sum of uniform interatomic potential may not represent the anisotropic and localized nature of the quantum trapping. The BOLS prediction has been confirmed by decoding the thermal stability and elasticity of SWCNT.[39]

**4.2. Charge Densification and Polarization.** Figure 2a illustrates the potential wells of quantum trapping at different atomic sites crossing a GNR. For atoms in the GNRs interior, the effective CN is reduced from the bulk value of 12 to 3, and the corresponding C−C bond length contracts to 81.5%, whereas at the edges, the atomic CN is 2 and the C−C bond contracts to 69.7%, according to the BOLS premise. The two- and three-coordinated C−C bond lengths have been confirmed in reproducing the thermal stability and elasticity of the SWCNT.[39] For the dangling bonds terminated by hydrogen, the C−H bond should be even shorter and stronger because of the CN that is even lower. Consequently, the density of the localized bonding electrons will increase with the inverse of the bond length from 1 unit to $0.815^{-1} = 1.22$ in the GNR interior and $0.6697^{-1} = 1.44$ near the edge, as compared with the charge density in a diamond.

On the other hand, the depth of the quantum-trapping potential well is proportional to the bond energy, $C_i^{-m}$. As illustrated in Figure 2a, the trap in the GNR interior is 1.69 times and at the edge it is 2.52 times deeper than the interatomic potential well in diamond if the bond nature indicator $m$ remains constant. Meanwhile, all the energy levels occupied by bonding electrons will go to deeper energies in the same $C_i^{-m}$ proportion, forming deeply and densely trapped local states. Figure 2b illustrates the polarization of the unpaired nonbonding electrons by the densely trapped bonding states. The densely and deeply trapped bonding electrons will polarize the unpaired nonbonding states that will eventually approach or even surpass the Fermi level, giving rise to the observed edge states in the vicinity of the Fermi energy. One can readily imagine the process of polarization and pinning of the unpaired nonbonding electron of a carbon atom by the three surrounding pairs of the sharing covalent electrons that are densified by bond contraction.

Figure 3 compares the energy states derived from the current DFT calculations. The edge states at the Fermi level are present in both the C−C atomic chain and the GNR, although the DOS feature in the C−C chain is less significant than that of the GNR. The calculated edge states are absent in other carbon materials, such as bulk diamond and LGS, because of the relatively lower portion of under-coordinated edge atoms. Although the calculated results manifest the BOLS expected trend of edge states, the exact extent of population is still far away from that expected

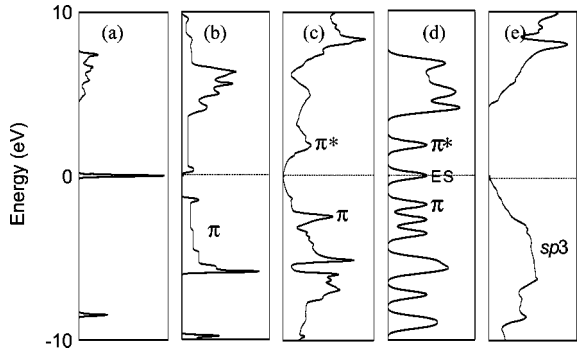


**Figure 3.** DFT calculation results of the density-of-states of carbon materials in different atomic CN: (a) single atom, (b) atomic chain, (c) infinite grapheme, (d) graphene nanoribbons, and (e) diamond. Parts b and d show the features of the edge states.

by BOLS correlation. As compared in Figure 1, the extent of C−C bond contraction does not follow the BOLS correlation well, in particular at lower atomic coordinations. As such, the calculated charge density is lower than the BOLS expectation. By taking the unusual edge boundary conditions into consideration (i.e., a potential barrier followed immediately by the deep potential trap), quantum calculations can produce the BOLS expected scenario.

Nevertheless, plenty of evidence has been reported for the BOLS expected strain and quantum trapping and the BOLS-derived $E_G$ expansion and core level shift. For instance, recent STM/S measurements and DFT computations[43] have revealed that the mean lattice constant of Co nanoislands contracts by 6% from the bulk value of 0.251 to 0.236 nm when one moves from the center to the edge of the nanoislands as the average atomic CN reduces. An apparent energy drop (∼0.2 eV) of the valence states has been detected using STS when the island size is reduced from 22.5 to 4.8 nm. For the silicon nanostructures, the $E_G$ expansion and the $E_{2p}$ level shift follow the same trend of BOLS anticipation.[44] At the lower end of the size limit ($K$ = 3) of a spherical Si dot, the $E_G$ expands by nearly 300% from 1.12 to 4.40 eV associated with an $E_{2p}$ level shift from the bulk value of −2.45 to −9.80 eV. It has been discovered[45] using STM/S at 4 K that the $E_G$ of Si nanorods increases from 1.1 to 3.5 eV when the rod diameter is decreased from 7.0 to 1.3 nm and that the surface Si−Si bond contracts by ∼12% from the bulk value 0.263 nm to ∼0.230 nm. This finding concurs exceedingly well with the BOLS expectation of a 200% $E_G$ expansion for the thinnest cylindrical rods of silicon. The consistency between the BOLS predicted and the experimentally observed $E_G$ expansion and core level shift of Co nanoislands and the nanostructured silicon evidence directly for the broken-bond-induced quantum trapping and the associated polarization of the antibonding states by the trapped bonding electrons. Therefore, as a rule, the broken bond, or the dangling bond, itself does not contrubute directly to the performance of a substance, but its effect on the remaining ones of the under-coordinated atoms is, indeed, profoundly significant. These findings evidence the reliability of the BOLS prediction in quantity on the CN dependence of bond length and the associated quantum trapping.

**4.3. Stiffness and Thermal Stability of SWCNT.** Quantitative information, such as the C−C bond dimension, elasticity, and thermal stability, gained from the massive amount of experimental data for SWCNT provides further evidence for the reliability of the BOLS correlation. The Young's modulus ($Y$) of the SWCNT was reported to vary from 0.5 to 5.5 TPa, depending on the presumed wall thickness. If one assumes the equilibrium interlayer spacing of a graphite sheet, $t_1$ = 0.34 nm, to represent the bond thickness, the derived $Y_1$ is ∼1.1 TPa.[46,47] If $t_1$ = 0.066 nm, which is close to the radius of a free C atom (∼0.0771−0.0914 nm), the $Y_1$ is derived as 5.5 TPa.[48] It is, however, surprising to find that the stiffness (or the product $Y_1t_1$) of the SWCNT approaches a constant of 0.3685 ± 0.0055 TPa·nm on the basis of a variety of observations. Recently, Lee et al.[49] measured the elastic properties and intrinsic breaking strength of a freestanding monolayer graphene by nanoindentation using an atomic force microscope. The intrinsic Young's modulus was determined as 1.05 TPa, on the basis of an assumption of an effective graphene thickness of 0.335 nm. The corresponding stiffness is 0.3517 TPa·nm, approaching the value for CNT. On the other hand, the STM tip end made of the SWCNT was observed to melt at 1593 K in ultrahigh vacuum,[50] which is far below the melting point of 3800 K for bulk diamond or graphite.

With the measured $Y_1t_1$ value of 0.3685 TPa·nm and the known temperature of the open-edge melting (1593 K) as input, we have determined the dimension and strength of a C−C bond in SWCNT, based on the relations of $Y_i \propto d_i^{-2}E_i$ and $T_{m,i} \propto z_iE_i$.[39] Considering atoms at sites of the open edge ($z_i$ = 2), wall interior ($z_i$ = 3), the graphite, and the diamond, we had a set of equatons. The unique solutions to these equations gave rise to the values of $m$ = 2.56 and the tube wall melting point, $T_{m,1}(3)$ = 1605 K. The C−C bond (or the wall of the SWCNT) thickness is 0.142 nm, with a $Y$ value that is 2.56 times the bulk value of 1.1 TPa. The C−C bond is 68% stronger than that in the bulk diamond. when comparing the derivative from the SWCNT to the measured graphene modulus of 1.05 TPa under the assumption of 0.335 nm thickness,[49] it is found that the elastic modulus of the graphene is 1.05 × 0.335/0.142 = 2.48 TPa, which is substantially the same as that of the SWCNT. The uniqueness of the solutions indicates that the BOLS scheme represents the true situations of observations as reported for the SWCNT and LGS. It is important to note that the nonbonding states play insignificant roles in determining the mechanical and thermal properties of the SWCNT and LGS. With the same approaches, we have reproduced the size-induced melting point depression and stiffness enhancement of a number of specimens, as discussed in detail in refs 26 and 29, evidencing the reliability of the BOLS scheme.

**4.4. Edge State Generation and Width Dependence of $E_G$ Expansion.** Figure 4a compares the calculated[6] and the measured[7] width dependence of $E_G$ expansion. The DFT calculations suggest that the $E_G$ of the AGNR expands from some 0.25 to 2.5 eV when the $K$ is decreased from 20 to 1.5, with the feature of 3$n$ periodicity.[6] Our AGNR calculation results in the range of the $K \leq 10$ repeat that is reported in ref 6. However, the conductance measurements revealed that the apparent $E_G$ increases from several milli-electron volts to 2.0 eV when the width of the GNR is decreased from $K$ = 40 to $K$ = 5. The measured data shows neither the DFT-derived 3$n$ oscillation nor orientation dependence. This inconsistency indicates clearly that the measurements in real situations and the calculations under ideal conditions are dominated by different mechanisms.

We attempted to reproduce the width dependence of the measured and the calculated $E_G$ by letting the $m$ value or the relative bond energy, $C_i^{-m}$, as a whole, change with the GNR

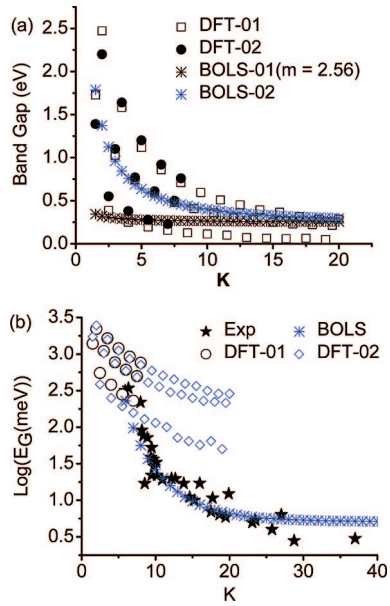


**Figure 4.** BOLS numerical fitting to the measured and the DFT-calculated width dependence of the band gap opening. (a) Three branches of gap variation by DFT-01 (see ref 6) and DFT-02 (current results) correspond to armchaired GNRs with $N = 3n$, $3n + 1$, and $3n + 2$ dimer chains across the width, where $n$ is a positive integer, which was ruled out in the measurement (see ref 8). (b) Comparison of the DFT and experimental results.[8] Numerical fit can be realized by employing a width dependence of the $m$ values, as discussed in the context. The DFT describes more intrinsic band gap under ideal conditions, whereas the experiment presents more on the apparent $E_G$ with the midgap impurity states being involved.

width. The two sets of data were fitted using the following expressions.

$$\begin{cases} E_G(K) & = E_G(\infty)[1 + \Delta(m)/(K - K_0)] \\ \Delta(m) & = \sum_{i\leq 3} C_i(C_i^{-m} - 1) \\ m & = m_0 + m_1/[1 + \exp((K - K_0)/K_l)] \end{cases} \quad (7)$$

An acceptable fit to the DFT results can be obtained with the highest $m$ value of 15.06 ($m_0 = 2.56$, $m_1 = 25$) at $K_0 = 1$ and $K_l = 20$. The maximal relative bond energy at the edge is $0.856^{-15.06} = 10.4$. For the experimental results, the highest $m$ value at $K_0 = 5$ is 27.56 with a $K_l$ value of 10; the corresponding relative bond energy is 72.6. Disregarding the inconsistency in fitting to both the theoretical and the experimental observations and the uncertainty in the derived $m$ values, on basis of the fitting, we can infer that the bond at the edge is at least 10 times stronger than that in the LGS. Such a huge bond-strength gain is beyond the expectation in numerical optimization using DFT or tight-binding approximations.

However, on the basis of the ideal case without the nonbonding states, we can estimate that the relative values of the band gap, the bandwidth, and the core level shift of the LGS with respect to the bulk diamond,

$$\frac{E_G(\text{GNR})}{E_G(\text{diamond})} = \frac{E_{\nu,\text{GNR}}}{E_{\nu,\text{diamond}}} = \frac{E_\nu(\text{GNR}) - E_\nu(1)}{E_\nu(\text{diamond}) - E_\nu(1)} = [C(3)]^{-2.56} = 1.69$$

the C−C bond in a LGS and in the SWCNT[39] is 0.69 times stronger than that in diamond. The band gap will expand from the diamond value of 5.50 to 9.29 eV if we turn the diamond into the LGS by removing the unpaired nonbonding electrons. The estimated $E_G$ value of 9.29 eV for the LGS is far beyond any observations. In fact, the LGS is gapless because of the involvement of the unpaired electrons.

By taking the effective atomic CN of atoms in the outermost two rows of the GNR as 2 and 2.5 and the subsequent row as 3, we obtained $C_1 = 0.695$, $C_2 = 0.767$, and $C_3 = 0.813$ with respect to the diamond bond length of 0.154 nm. Substituting $C_1/C_3 = 0.856$ and $C_2/C_3 = 0.941$ for the $C_1$ and $C_2$ values in eq 6 referring to a GNR with the constant $m = 2.56$, the factor of enhancement is estimated as

$$\frac{E_G(K)}{E_G(\infty)} = \frac{E_\nu(K) - E_\nu(1)}{E_\nu(\infty) - E_\nu(1)} = 1 + \frac{1}{K}\sum_{i\leq 3} C_i(C_i^{-2.56} - 1) = 1 + 0.577K^{-1} \quad (8)$$

The maximal $E_G$ of the GNR is estimated to be $9.29(1 + 0.577) = 14.66$ eV at $K = 1$, if the unpaired electrons are absent. Correspondingly, the maximal depth of the trapping potential well of the GNR is estimated at $1.69 \times 1.57 = 2.65$ times that of a diamond, being independent of the GNR orientation.

**4.5. Significance of Nonbonding States.** It is unexpectedly surprising that the BOLS, the DFT, and the experimentally measured results are different one from another. Although we have reproduced the size dependence of the thermal stability, mechanical strength, band gap, and core level shift of numerous specimens,[26] including the SWCNT and the nanostructured silicon, the BOLS appears uncertain for the $E_G$ of the GNRs.

The inconsistency discussed above indicates, however, the impact of the nonbonding midgap states and the inhomogeneous stress caused by edge chemisorption, which can hardly be represented at the present in theoretical computations. The nonbonding states dominate the apparent $E_G$ because one can measure transition of electrons from the midgap nonbonding states to the tail of the conduction band rather than from the valence band to the conduction band directly if the midgap states are present.[31] From this point of view, the experiments measure the true, but not the intrinsic, $E_G$ because of the presence of the midgap nonbonding states. The measured trend of $E_G$ expansion instead gives information about the change of the separation between the upper edge of nonbonding states and the conduction band tail.

**4.6. Effect of Edge Adsorption.** It is noted that the ideal ZGNR is originally metallic with a smaller $E_G$ and apparent edge states, whereas the AGNR is a semiconductor with a wider $E_G$ and insignificant edge states. According to eq 1, neither the $E_G$ nor the core-level shift is orientation-dependent if the nonbonding states or the stress induced by edge adsorption is excluded. Figure 5 illustrates the edge termination by hydrogen atoms. Due to charge repopulation in the chemisorption, the H atom will not be neutral because it carries a certain amount of charge. The repulsion along the −H−H−H− chain cannot be

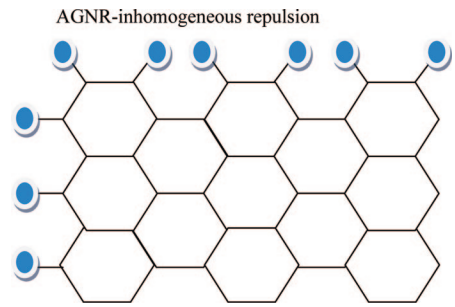


**Figure 5.** Illustration of the homogeneous/inhomogeneous repulsion along the edges of the ZGNR/AGNR, which may distinguish them one from another.

neglected. Along the edge of the ZGNR, no additional force will be acting on the carbon atoms; however, inhomogeneous force will act on the carbon atoms along the AGNR edges, which will cause lattice relaxation and, hence, interatomic bonding energy weakening. Therefore, the intrinsic $E_G$ and the potential depth at the edge of the AGNR is expected to be weakened as compared with the ideal values that ZGNR retain. The relatively deeper potential of the ZGNR expels the nonbonding states, giving rise to the pronounced edge states' demonstrating metallic behavior. However, the relatively shallower potential in the AGNR edge will weaken the edge states exhibiting semiconductive nature. Therefore, the presence and polarization of the nonbonding states and the inhomogeneous stress along the two different edges cause the orientation-induced difference.

**4.7. Brillouin Zone and Dispersion Relation.** It is anticipated that as the bond contracts in the GNRs, the reciprocal lattice and the Brillouin zone will expand by $C_i^{-1}$ ($\sim$1.4), and the bandwidth will also expand by $C_i^{-m}$ (2.56 at edges). This reciprocal reconfiguration will stretch the dispersion relation $E_\nu(K)$ with linearization. As we know, the dispersion curve determines the effective mass, $\hbar^2[\nabla_k^2 E_\nu(k)]^{-1}$, and the group velocity, $\nabla_k E_\nu(k)/\hbar$, of the bonding electrons. The stretch and linearization of the dispersion may result in a constant $\nabla_k E_\nu(k)$ and a nearly zero $\nabla_k^2 E_\nu(k)$, which leads to the lower group velocity and infinity effective mass. However, the mass and velocity of the unpaired nonbonding electrons located at the corner of the Brillouin zone of the GNRs may not follow this expectation. The almost zero mass and infinite velocity of charge should refer to the nonbonding $\pi$-electron Dirac states rather than the bonding electrons that follow the stretched dispersion curve.

## V. Conclusion

We have established the relationship among the elastic modulus, thermal stability, band structure, and the edge states of GNRs through the BOLS correlation and the local bond average approach. The elastic modulus is proportional to the energy density, and the band gap is proportional to the bond energy or the interatomic potential in the Hamiltonian. An incorporation of the BOLS correlation to the DFT calculations and experimental observations has led to consistent insight into the physical origin of the generation of the strongly localized edge states and the expansion of the band gap of GNRs. The consistency between BOLS expectations and the observed coordination dependence of bond contraction and the associated thermal instability and stiffness enhancement in various situations, including the SWCNT, evidence the significance of the broken bonds that induce strain and quantum trapping. The inconsistency between the theoretically and experimentally observed band gap expansions in GNRs indicates the impact of the unpaired nonbonding states. It is understood that a perturbation to the Hamiltonian by the broken-bond-induced bond strain and quantum trapping causes the band gap expansion and the core level shift and that the polarization of the unpaired nonbonding states by the strongly localized and deeply trapped bonding electrons is responsible for the observed edge states in GNRs. The difference between the AGNR and the ZGNR in electronic structure arises from the adsorbate-induced inhomogeneous repulsion along the edges, because the intrinsic band structure depends neither on the geometrical orientation nor on the presence of nonbonding states. The understanding herewith and the previously reported findings may extend to other situations with a large proportion of under-coordinated atoms, such as the densification and localization of electrons with lowered binding energy in the potential traps as observed as defect states,[51] chain end states,[52,53] terrace edge states,[54,55] and surface states.[56−58] The broken bonds do not contribute directly to the performance of a specimen, but its consequence on the remaining ones does indeed have enormous impact on the low-dimensional systems. The combination of the broken bonds and the unpaired nonbonding states is, indeed, fascinating. Findings will inspire further interest in low-dimensional materials from the perspective of bond formation, dissociation, relaxation, vibration, and the associated geometric and energetic response of the bonds to the bonding environment and the densification, localization, and polarization of the bonding and nonbonding electrons.

**Acknowledgment.** Financial support from MOE (Grants ARC 03/07, ARC 04/06, and RG14/06) of Singapore; NSF (Grant no. 10772157) of China; and the KC Wong Foundation, Hong Kong, is gratefully acknowledged.

## References and Notes

(1) Hiura, H. *Appl. Surf. Sci.* **2004**, *222*, 374.
(2) Fujita, M.; Wakabayashi, K.; Nakada, K.; Kusakabe, K. *J. Phys. Soc. Jpn.* **1996**, *65*, 1920.
(3) Novoselov, K. S.; Geim, A. K.; Morozov, S. V.; Jiang, D.; Zhang, Y.; Dubonos, S. V.; Grigorieva, I. V.; Firsov, A. A. *Science* **2004**, *306*, 666.
(4) Ohta, T.; Bostwick, A.; Seyller, T.; Horn, K.; Rotenberg, E. *Science* **2006**, *313*, 951.
(5) Nakada, K.; Fujita, M.; Dresselhaus, G.; Dresselhaus, M. S. *Phys. Rev. B* **1996**, *54*, 17954.
(6) Son, Y.-W.; Cohen, M. L.; Louie, S. G. *Phys. Rev. Lett.* **2006**, *97*, 216803.
(7) Gunlycke, D.; White, C. T. *Phys. Rev. B* **2008**, *77*, 115116.
(8) Han, M. Y.; Özyilmaz, B.; Zhang, Y. B.; Kim, P. *Phys. Rev. Lett.* **2007**, *98*, 206805.
(9) Yu, S. S.; Wen, Q. B.; Zheng, W. T. *Mol. Simul.* **2008**, in press.
(10) Finkenstadt, D.; Pennington, G.; Mehl, M. J. *Phys. Rev. B* **2007**, *76*, 121405.
(11) Gunlycke, D.; Areshkin, D. A.; White, C. T. *Appl. Phys. Lett.* **2007**, *90*, 142104.
(12) Li, T. C.; Lu, S. P. *Phys. Rev. B* **2008**, *77*, 085408.
(13) Kan, E.-J.; Li, Z. Y.; Yang, J. L.; Hou, J. G. *J. Am. Chem. Soc.* **2008**, *130*, 4224.
(14) Yu, S. S.; Wen, Q. B.; Zheng, W. T.; Jiang, Q. *Carbon* **2008**, *46*, 537.
(15) Enoki, T.; Kobayashi, Y.; Fukui, K.-I. *Int. Rev. Phys. Chem.* **2007**, *26*, 609.
(16) Zhang, Y.; Tan, J. W.; Stormer, H. L.; Kim, P. *Nature* **2005**, *438*, 201.
(17) Bolotin, K. I.; Sikes, K. J.; Jiang, Z.; Klima, M.; Fudenberg, G.; Hone, J.; Kim, P.; Stormer, H. L. *Solid State Commun.* **2008**, *146*, 351.
(18) Ghosh, S.; Calizo, I.; Teweldebrhan, D. C.; Pokatilov, E. P.; Nika, D. L.; Balandin, A. A.; Bao, W.; Miao, F.; Lau, C. N. *Appl. Phys. Lett.* **2008**, *92*, 151911.
(19) Nano Letters, in press, DOI: 10.1021/nl0731872 Balandin, A. A.; Ghosh, S.; Bao, W.; Calizo, I.; Teweldebrhan, D.; Miao, F.; Lau, C. N. *Nano Lett.* **2008**, *8*, 902.
(20) Bullis, K. Graphene Transistors, Technology Review; MIT Technology Review: Cambridge, 2008.
(21) Rotenberg, E.; Bostwick, A.; Ohta, T.; McChesney, J. L.; Seyller, T.; Horn, K. *Nat. Mater.* **2008**, *7*, 258.
(22) Zanella, I.; Guerini, S.; Fagan, S. B.; Mendes Filho, J.; Souza Filho, A. G. *Phys. Rev. B* **2008**, *77*, 073404.
(23) Zhou, S. Y.; Siegel, D. A.; Fedoro, A. V.; Gabaly, F. E.; Schmid, A. K.; Castro Neto, A. H.; Lee, D. H.; Lanzara, A. *Nat. Mater.* **2008**, *7*, 259.
(24) Zhou, S. Y.; Gweon, G.-H.; Fedorov, A. V.; First, P. N.; de Heer, W. A.; Lee, D. H.; Guinea, F.; Castro Neto, A. H.; Lanzara, A. *Nat. Mater.* **2007**, *6*, 770.
(25) Kane, C. L.; Mele, E. J. *Phys. Rev. Lett.* **2005**, *95*, 146802.
(26) Sun, C. Q. *Prog. Solid State Chem.* **2007**, *35*, 1.
(27) Omar, M. A. *Elementary Solid State Physics: Principles and Applications*; Addison-Wesley: New York, 1993.
(28) Sun, C. Q. *Phys. Rev. B* **2004**, *69*, 045105.
(29) Sun, C. Q. *Prog. Mater. Sci.* **2008**, in press, DOI: 10.1016/j.pmatsci.2008.08.001.
(30) Sun, C. Q. *Prog. Mater. Sci.* **2003**, *48*, 521.

(31) Street, R. A. *Hydrogenated Amorphous Silicon*; Cambridge University Press: Cambridge, 1991.
(32) Atkins, P. W. *Physical Chemistry*, 4th ed.; Oxford University Press: Oxford, 1990; p 409.
(33) Zheng, W. T.; Sun, C. Q. *Prog. Solid State Chem.* **2006**, *34*, 1.
(34) Goldschmidt, W. T. *Ber. Deut. Chem. Ges.* **2007**, *60*, 1270.
(35) Pauling, L. *J. Am. Chem. Soc.* **1947**, *69*, 542.
(36) Feibelman, P. J. *Phys. Rev. B* **1996**, *53*, 13740.
(37) Huang, W. J.; Sun, R.; Tao, J.; Menard, L. D.; Nuzzo, R. G.; Zuo, J. M. *Nat. Mater.* **2008**, *7*, 308.
(38) Miller, J. T.; Kropf, A. J.; Zha, Y.; Regalbuto, J. R.; Delannoy, L.; Louis, C.; Bus, E.; van Bokhoven, J. A. J. *Catalysis* **2006**, *240*, 222.
(39) Sun, C. Q.; Bai, H. L.; Tay, B. K.; Li, S.; Jiang, E. Y. *J. Phys. Chem. B* **2003**, *107*, 7544.
(40) Sun, C. Q.; Li, C. M.; Bai, H. L.; Jiang, E. Y. *Nanotechnology* **2005**, *16*, 1290.
(41) Delley, B. *J. Chem. Phys.* **1990**, *92*, 508.
(42) Perdew, J. P.; Burke, K.; Ernzerhof, M. *Phys. Rev. Lett.* **1996**, *77*, 3865.
(43) Mironets, O.; Meyerheim, H. L.; Tusche, C.; Stepanyuk, V. S.; Soyka, E.; Zschack, P.; Hong, H.; Jeutter, N.; Felici, R.; Kirschner, J. *Phys. Rev. Lett.* **2008**, *100*, 096103.
(44) Sun, C. Q.; Pan, L. K.; Fu, Y. Q.; Tay, B. K.; Li, S. *J. Phys. Chem. B* **2003**, *107*, 5113.
(45) Ma, D. D. D.; Lee, C. S.; Au, F. C. K.; Tong, S. Y.; Lee, S. T. *Science* **2003**, *299*, 1874.
(46) Wong, E. W.; Sheehan, P. E.; Lieber, C. M. *Science* **1997**, *277*, 1971.
(47) Falvo, M. R.; Clary, G. J.; Taylor, R. M., II; Chi, V., Jr.; Washburn, S.; Superfine, R. *Nature (London)* **1997**, *389*, 582.
(48) Yakobson, B. I.; Brabec, C. J.; Bernholc, J. *Phys. Rev. Lett.* **1996**, *76*, 2511.
(49) Lee, C.; Wei, X.; Kysar, J. W.; Hone, J. *Science* **2008**, *321*, 385.
(50) An, B.; Fukuyama, S.; Yokogawa, K.; Yoshimura, M. *Jpn. J. Appl. Phys.* **1998**, *37*, 3809.
(51) Niimi, Y.; Matsui, T.; Kambara, H.; Fukuyama, H. *Phys. E* **2006**, *34*, 100.
(52) Stepanyuk, V. S.; Klavsyuk, A. N.; Niebergall, L.; Bruno, P. *Phys. Rev. B* **2005**, *72*, 153407.
(53) Crain, J. N.; Pierce, D. T. *Science* **2005**, *307*, 703.
(54) Kobayashi, Y.; Kusakabe, K.; Fukui, K.; Enoki, T. *Phys. E* **2006**, *34*, 678.
(55) Mattila, S.; Leiro, J. A.; Heinonen, M.; Laiho, T. *Surf. Sci.* **2006**, *600*, 1168.
(56) Eguchi, T.; Kamoshida, A.; Ono, M.; Hamada, M.; Shoda, R.; Nishio, T.; Harasawa, A.; Okuda, T.; Kinoshita, T.; Hasegawa, Y. *Phys. Rev. B* **2006**, *74*, 073403.
(57) Ciston, J.; Marks, L. D.; Feidenhans'l, R.; Bunk, O.; Falkenberg, G.; Lauridsen, E. M. *Phys. Rev. B* **2006**, *74*, 085401.
(58) Fauster, T.; Reu$\beta$, Ch.; Shumay, I. L.; Weinelt, M.; Theilmann, F.; Goldmann, A. *Phys. Rev. B* **2000**, *61*, 16168.

JP807580T